Phytopathology • 2020 • 110:1530-1540 • https://doi.org/10.1094/PHYTO-04-20-0114-R

Mycology

e-Xtra*

# Molecular Characterization of the Purine Degradation Pathway Genes *ALA1* and *URE1* of the Maize Anthracnose Fungus *Colletotrichum graminicola* Identified Urease as a Novel Target for Plant Disease Control

Elvio Henrique Benatto Perino,[1] Chirlei Glienke,[1,2,†] Alan de Oliveira Silva,[1,2] and Holger B. Deising[2,†]

[1] Postgraduate Program in Genetics, Department of Genetics, Federal University of Paraná, Centro Politécnico, Jardim das Américas, 81531-990, Curitiba, Paraná State, Brazil

[2] Martin Luther University Halle-Wittenberg, Faculty of Natural Sciences III, Institute for Agricultural and Nutritional Sciences, Chair for Phytopathology and Plant Protection, Betty-Heimann-Str. 3; D-06120 Halle (Saale), Germany

Accepted for publication 27 April 2020.

## ABSTRACT

Fungal pathogenicity is governed by environmental factors, with nitrogen playing a key role in triggering pathogenic development. Spores germinating on the plant cuticle are exposed to a nitrogen-free environment, and reprograming of nitrogen metabolism is required for bridging the time needed to gain access to the nitrogen sources of the host. Although degradation of endogenous purine bases efficiently generates ammonium and may allow the fungus to bridge the preinvasion nitrogen gap, the roles of the purine degradation pathway and of the key genes encoding allantoicase and urease are largely unknown in plant pathogenic fungi. To investigate the roles of the allantoicase and urease genes *ALA1* and *URE1* of the maize anthracnose fungus *Colletotrichum graminicola* in pathogenic development, we generated *ALA1*:*eGFP* and *URE1*:*eGFP* fusion strains as well as allantoicase- and urease-deficient mutants. Virulence assays, live cell, and differential interference contrast imaging, chemical complementation and employment of a urease inhibitor showed that the purine degradation genes *ALA1* and *URE1* are required for bridging nitrogen deficiency at early phases of the infection process and for full virulence. Application of the urease inhibitor acetohydroxamic acid did not only protect maize from *C. graminicola* infection, but also interfered with the infection process of the wheat powdery mildew fungus *Blumeria graminis* f. sp. *tritici*, the maize and broad bean rusts *Puccinia sorghi* and *Uromyces viciae-fabae*, and the potato late blight pathogen *Phytophthora infestans*. Our data strongly suggest that inhibition of the purine degradation pathway might represent a novel approach to control plant pathogenic fungi and oomycetes.

*Keywords*: acetohydroxamic acid, allantoicase, ammonium, appressorial penetration, biochemistry and cell biology, disease control and pest management, mycology, nitrogen limitation, novel plant health strategy, powdery mildew, *Phytophthora*, rust, urease

Propagules of pathogenic fungi infecting above-ground plant organs land on and adhere to the hydrophobic epicuticular wax layer. Hydrophobicity, topography, and wax fatty alcohol composition of the plant surface contribute to host recognition, initiation of infection structure differentiation, and hence, pathogenesis (Lee and Dean 1994; Mendgen and Deising 1993; Podila et al. 1993). Analytical chemistry showed that epidermal cell wall appositions are basically devoid of nitrogen (Buschhaus and Jetter 2011; Podila et al. 1993). Depending on the lifestyle of plant pathogens, nitrogen limitation may serve as a signal required for initiation of the infection process. In vegetative hyphae of the rice blast fungus *Magnaporthe oryzae*, nitrogen starvation stress induced the expression of genes normally expressed during fungal in planta growth and has been considered as one of the inductive cues for disease symptom expression (Talbot et al. 1997). In several necrotrophic plant pathogens, nitrogen starvation activates secondary metabolism gene clusters and formation of toxins (Tudzynski 2014, and references therein). Illustrating the potency of toxins, one single germinating spore of the necrotrophic pear pathogen *Alternaria kikuchiana* releases amounts of the host-specific AK toxin sufficient to disrupt membrane integrity of approximately 100 host cells prior to host invasion (Nishimura and Kohmoto 1983). Likely, membrane disintegration does not only cause electrolyte leakage but also provides the fungus with nitrogen-containing compounds at very early stages of pathogenesis. In contrast, hemibiotrophs and biotrophs do not disrupt the host plasma membrane and thus have a severely extended phase of nitrogen limitation. Hemibiotrophic *Colletotrichum* species such as the maize anthracnose fungus *Colletotrichum graminicola* or the *Brassica* pathogen *C. higginsianum* (Bergstrom and Nicholson 1999; O'Connell et al. 2012) differentiate melanized appressoria, forcefully invade the first host epidermal cell (Bechinger et al. 1999; Ludwig et al. 2014) and invaginate the plasma membrane of their host (Kankanala et al. 2007; Kleemann et al. 2012; Politis and Wheeler 1973). Likewise, haustoria of obligate biotrophs invaginate the plasma membrane of their hosts and thus haustoria and biotrophic hyphae of hemibiotrophs remain localized in the plant apoplast (Kleemann et al. 2012; Kwaaitaal et al. 2017; Voegele and Mendgen 2003). Thorough analyses in oilseed rape (*Brassica napus*) have shown that the ammonium concentration of the leaf

†Corresponding authors: C. Glienke; ch.glienke@gmail.com, and H. B. Deising; holger.deising@landw.uni-halle.de

Current address of E. H. Benatto Perino: Leibniz-Institute of Plant Biochemistry (IPB), Weinberg 3, D-06120 Halle (Saale), Germany.

**Funding:** This study was supported by Coordenação de Aperfeiçoamento de Pessoal de Nível Superior (CAPES/PROAP Finance Code 001), Conselho Nacional de Desenvolvimento Científico e Tecnológico (CNPq) (424738/2016-3 and 309971/2016-0), INCT Citros (CNPq573848/08-4) and Fundação Araucária de Apoio ao Desenvolvimento Científico e Tecnológico do Estado do Paraná. We thank CAPES for scholarships awarded to E. H. Benatto Perino and A. de Oliveira Silva, and CNPq for a scholarship for C. Glienke (200976/2014-1). The European Social Fund (ESF) provided support for the International Graduate School AGRIPOLY–Determinants of Plant Performance (grant ZS/2016/08/80644 to H. B. Deising, project "Chromatin modification in fungal pathogenicity").

*The *e-Xtra* logo stands for "electronic extra" and indicates that four supplementary figures and one supplementary table are published online.

The author(s) declare no conflict of interest.

apoplast depends on the nutritional status of the plant but rarely exceeds the micromolar range (Schjoerring et al. 2002). For comparison, media optimized for vegetative hyphal growth of *Aspergillus nidulans* contain approximately 70 mM ammonium (Käfer 1977). The ammonium requirement of biotrophic hyphae is difficult to address and therefore as yet unknown, but one may assume that micromolar ammonium concentrations do not represent a satisfactory nitrogen reservoir for these hyphae.

Thus, due to nitrogen starvation, effective nitrogen reallocation appears to be required during on *planta* appressorium differentiation and in biotrophic hyphae. Indeed, in *M. oryzae* high-throughput super serial analysis of gene expression identified increased transcript abundances of 1,026 genes during appressorium development and of 1,492 genes during appressorium maturation (Soanes et al. 2012), suggesting a significant demand for ammonium in de novo synthesis of nucleotides and amino acids in transcriptional and translational reprogramming at this stage of pathogenesis. RNA sequencing has also shown that formation of biotrophic hyphae of *C. higginsianum* and *C. graminicola* in the apoplast is associated with significant deregulation of 377 and 440 genes, respectively (O'Connell et al. 2012), indicating continuing nitrogen reallocation during biotrophy. Surprisingly, in spite of the obvious importance of this process, mechanisms of nitrogen reallocation in fungi at early stages of pathogenesis are poorly understood.

In apoplasts of tomato leaves infected by the biotroph *Cladosporium fulvum*, plant-derived γ-amino butyric acid and uric acid accumulate and are thought to contribute to the plant reactive oxygen scavenger-based defense system. In *Fusarium oxysporum* infecting tomato, urate oxidase (syn. uricase) (Supplementary Fig. S1), an enzyme converting uric acid to allantoin, was induced at stages preceding necrotrophy, suggesting that the pathogen highjacks these nitrogen-rich plant reactive oxygen species scavenging compounds in order to overcome nitrogen insufficiency (Divon and Fluhr 2007). Direct genetic evidence supporting the hypothesis that degradation of endogenous fungal purines is required for bridging the nitrogen availability gap occurring on the plant cuticle came from random *Agrobacterium tumefaciens*-mediated mutagenesis experiments in *C. graminicola* (Münch et al. 2011). One of the mutants, designated as AT171, carried a T-DNA insertion 88-bp upstream of the start codon of the allantoicase gene, i.e., likely within the promoter region (Münch et al. 2011). In agreement with the hypothesis that defects in purine degradation would cause severe nitrogen limitations at prepenetration and early biotrophic stages of the infection process, mutant AT171 exhibited appressorial penetration and virulence defects. These observations suggest that nucleotides and amino acids resulting from transcript and protein degradation are not sufficient to bridge the nitrogen deficiency gap occurring at early stages of pathogenesis, making liberation of ammonium through purine degradation indispensable for nitrogen reallocation and full virulence.

Following conversion of purine bases to allantoin, formation of allantoate is catalyzed by the enzyme allantoinase (Supplementary Fig. S1) (Lee et al. 2013). Allantoicase then cleaves allantoate, yielding urea and (*S*)-ureidoglycolate, both of which contain two nitrogen atoms. Using the latter molecule as a substrate, the enzyme ureidoglycolate hydrolase generates a second molecule of urea and liberates glyoxylate. Both urea molecules are then converted to ammonium by the enzyme urease. This pathway thus yields four moles of ammonium per mole of purine base (Supplementary Fig. S1) (Lee et al. 2013), making it ideally suited for bridging the nitrogen availability gap at early stages of the infection process. In a side-branch, a transamination reaction catalyzed by the enzyme (*S*)-ureidoglycine-glyoxylate aminotransferase, the substrate (*S*)-ureidoglycine provides both the amino group donor and the amino group acceptor glyoxylate, resulting in formation of the amino acid glycine (Supplementary Fig. S1) and connecting purine degradation with amino acid biosynthesis (Ramazzina et al. 2010). Although transcript abundances may not directly reflect metabolite fluxes, the 13- and 18-fold allantoicase transcript abundance in appressoria and biotrophic hyphae, as compared with allantoate amidohydrolase transcript abundance (O'Connell et al. 2012), suggests that a direct nitrogen flow through (*S*)-ureidoglycine into glycine is of minor importance. In addition, these transcript abundance data imply that the enzymes allantoicase and urease are key enzymes in ammonium generation at early phases of fungal pathogenic development.

In order to analyze the role of the purine degradation pathway, we generated *eGFP*-fusion strains and allantoicase- and urease-deficient mutants of *C. graminicola* by homologous recombination. Virulence assays, live cell and differential interference contrast (DIC) imaging, chemical complementation and inhibition of urease showed that the purine degradation pathway significantly contributes to virulence of *C. graminicola*. Intriguingly, a urease inhibitor did not only reduce the severity of maize anthracnose disease symptoms, but also protected crops from powdery mildew, rust, and oomycete infections. Our studies strongly suggest that interference with the purine degradation pathway might be a novel approach to control plant pathogenic fungi and oomycetes.

## MATERIALS AND METHODS

**Fungal and plant material, and infection assays.** The wild-type (WT) strain CgM2 (syn. M.1.001) of *C. graminicola* (teleomorph *Glomerella graminicola*) was a gift from Ralph L. Nicholson, Purdue University, Indiana, U.S.A., and maintained on oatmeal agar at 23°C as described (Sugui and Deising 2002). The wheat powdery mildew fungus *Blumeria graminis* f. sp. *tritici* was a field isolate (BgtEV01) collected at the experimental station of Martin Luther University and maintained on susceptible wheat plants in a green house at 21 ± 1°C. The broad bean rust fungus *Uromyces viciae-fabae* and the maize rust fungus *Puccinia sorghi* were gifts from Kurt Mendgen, University of Constance, Germany. Urediniospores were stored at –78°C until needed. The potato late blight oomycete strain CRA208m2 of *Phytophthora infestans* (Si-Ammour et al. 2003) was a gift from Sabine Rosahl, Leibniz Institute of Plant Biochemistry, Halle (Saale), Germany. Zoospore suspensions of *Phytophthora infestans* were prepared as described (Eschen-Lippold et al. 2007).

Plants used in infection experiments were maize (*Zea maize* 'Mikado'; KWS SAAT SE), winter wheat (*Triticum aestivum* 'Winnetou'; Saatzucht Firlbeck GmbH & Co. KG), broad bean (*Vicia faba* 'Fuego'; Norddeutsche Pflanzenzucht Hans-Georg Lembke KG, Germany), and potato (*Solanum tuberosum* L. 'Désirée') (Halim et al. 2007). Potato plants were propagated at the Institute for Plant Biochemistry, Halle (Saale), Germany, kindly provided by Sabine Rosahl, and grown at 21 ± 1°C with a 16-h light period. The photon flux was ~140 µmol/m$^2$/s, except for *Z. mays*, which was grown at ~300 µmol/m$^2$/s).

Conidia of *C. graminicola* that had formed on Petri dishes at 14 days postinoculation (dpi) were suspended in distilled $H_2O$ containing 0.02% (vol/vol) Tween 20 and adjusted to a concentration of $10^6$ conidia/ml to study symptom severity or $10^5$ conidia/ml for microscopy. Leaves were inoculated using 10 µl droplets as described (Horbach et al. 2009). For rust inoculations, 25 ml of suspensions containing 0.1 mg of urediniospores per ml of 0.02% (vol/vol) Tween 20 per plant was sprayed onto the lower epidermis of leaves. Plants were incubated in darkness for 24 h at 22°C and 100% relative humidity and returned to 16 h light period as described above. Mildew inoculation was performed by dusting conidia onto plants, using strongly infected wheat plants as the inoculum, and plants were incubated as described for rust-inoculated plants. For *Phytophthora infestans* infections, lower leaves were drop inoculated with a zoospore suspension in water ($1 \times 10^5$ zoospores/ml) on the abaxial leaf surface and kept at 100%

humidity for 24 h (Eschen-Lippold et al. 2007). For chemical complementation, inoculation droplets were adjusted to contain 10 mM $(NH_4)_2SO_4$. For urease inhibitor treatment, the spore suspensions of *C. graminicola*, rust species and zoospore suspensions of *Phytophthora infestans* were adjusted to contain 10 mM of acetohydroxamic acid (AHA; Sigma-Aldrich, Darmstadt, Germany). To test the effect of AHA on mildew infection, 10 mM of the inhibitor was sprayed onto leaves to the point of run-off and allowed to dry for 4 h. Mildew inoculation was performed and subsequently cultivated as described above. Disease symptom development was observed and photographed daily. To analyze the effect of AHA on *C. graminicola* infection structure differentiation, leaves were harvested at 1 and 2 dpi, bleached in acetate-ethanol (1:3, vol/vol) overnight and subjected to microscopy. To analyze the effect of AHA on rust infection structure differentiation, urediniospores of *U. viciae-fabae* were suspended in 10 mM AHA in 0.02% (vol/vol) Tween 20 and sprayed onto thigmo-inductive polyethylene sheets (Deising et al. 1991). Infection structures were stained with methyl blue (Sigma-Aldrich) (de Neergaard 1997), photographed, and counted at 24 h postinoculation (hpi). AHA (10 mM) was used to analyze phytotoxicity.

**Generation of *eGFP* strains and targeted mutagenesis.** *Generation of* eGFP *strains.* To study infection structure-specific expression of *ALA1* and *URE1*, *eGFP* fusion cassettes were constructed and transformed into the *C. graminicola* WT strain. The *ALA1*:*eGFP* fusion cassette consisted of the 952-bp 3′-end of the coding region of the *ALA1* gene without the stop codon, and fused in frame to the *eGFP* gene lacking the start codon, followed by the hygromycin B resistance gene and the noncoding 730-bp 3′-flank of *ALA1* containing the terminator (Supplementary Fig. S2A). The *URE1*:*eGFP* fusion cassette consisted of the 1,007-bp 3′-end of the coding region of the *URE1* gene without the stop codon, fused in frame to the *eGFP* gene lacking the start codon, followed by the G418 resistance gene and the noncoding 955-bp 3′-flank of *URE1*, containing the terminator (Supplementary Fig. S2C).

In detail, the 3′-coding region of *ALA1* was amplified with the primers CgAlaGfp-fw and CgAlaGfp-rv (all primers used in this study are given in Supplementary Table S1), and the 3′-coding region of *URE1* was amplified using primers CgUreGfp-fw and CgUreGfp-rv, and *C. graminicola* genomic DNA as template. The *eGFP* gene fused to the hygromycin resistance cassette was amplified using primers GfpFusion-fw and GfpHygFusion-rv, with plasmid pSH1.6EGFP, kindly provided by Amir Sharon, Tel Aviv University, Israel, as template. The *eGFP* gene fused to the Geneticin (G418) resistance gene was amplified using primers GfpFusion-fw and GfpG418Fusion-rv, and plasmid pGG-14, provided by Diana Gottschling and Fabian Weihmann, MLU Halle, Germany, as template. Using *C. graminicola* genomic DNA as template, the 3′-noncoding sequence of *ALA1*, containing the terminator, was amplified with primers CgTala1-fw and CgTala1-rv2, and the 3′-noncoding sequence of *URE1*, containing the terminator, was amplified with primers CgTureGfpFusion-fw and CgTure1-rv, using genomic DNA of *C. graminicola* as the template. The *ALA1:eGFP* and *URE1:eGFP* cassettes were fused by double-joint PCR (Yu et al. 2004), and the complete 5,230- and 4,527-bp *ALA1:eGFP* and *URE1:eGFP* cassettes were amplified using the nested primers pairs CgAla1Gfp1Nested-fw and CgAla1Gfp1Nested-rv, and CgUre1Gfp1Nested-fw and CgUre1Gfp1Nested-rv, respectively. Phusion high-fidelity DNA polymerase (New England Biolabs, Frankfurt a.M., Germany) was used in all PCR reactions. The *ALA1:eGFP* and *URE1:eGFP* cassettes were transformed into protoplasts generated from oval conidial (Werner et al. 2007).

The correct integration of a single copy of the *eGFP* fusion constructs at the 3′-ends of the coding regions of *ALA1* and *URE1* was confirmed by genomic Southern hybridization (Brown 1999). Ten micrograms of genomic DNA (Sugui and Deising 2002) of the WT and eGFP-fusion strains were digested with restriction endonuclease *Bgl*II for *ALA1*:*eGFP*, and *Xho*I for *URE1*:*eGFP*. Digested DNA was separated on 0.7% (wt/vol) TAE agarose gels, and depurinated DNA was blotted onto nylon membranes (Hybond-N+; Amersham Pharmacia Biotech, Freiburg am Breisgau, Germany) (Brown 1999). DNA was denatured in 0.5 M NaOH and hybridized with 474- and 480-bp DIG-dUTP-labeled hygromycin-B phosphotransferase (*hph*)- and *G418*-specific probes, respectively (Supplementary Fig. S2A and C). The alkali-labile DIG-dUTP-labeled (Roche Diagnostics, Mannheim, Germany) *hph*-specific probe was amplified from plasmid pAN7-1 (Punt et al. 1987), using primers HygRprobe-fw and HygRprobe-rv. The *G418*-specific probe was amplified from plasmid pGG-14, using primers CgGenProbe-fw2 and CgGenProbe-rv2.

*Targeted gene deletion.* In order to delete the 1,130-bp *ALA1* and the 2,832-bp *URE1* gene of *C. graminicola*, the hygromycin-B phosphotransferase (*hph*) gene from *Escherichia coli* was PCR-amplified from pAN7-1 (Punt et al. 1987), using primers Hyg-fw and Hyg-rv. The 1,000-bp 5′- and the 730-bp 3′-flanks of *ALA1* were amplified from *C. graminicola* genomic DNA using primers CgPala1-fw and CgPala1-rv, and CgTala1-fw and CgTala1-rv, respectively. Correspondingly, the 941-bp 5′- and the 976-bp 3′-flanking regions of the *URE1* gene were amplified from genomic DNA using primers CgPure1-fw and CgPure1-rv, and CgTure1-fw and CgTure1-rv. The 5′- and 3′-flanks were fused with the *HPH* cassette by DJ-PCR (Yu et al. 2004), and nested primers CgPala1nest-fw and CgTala1nest-rv were then used to amplify the 3,739-bp allantoicase deletion cassette (Supplementary Fig. S4A). Likewise, primers CgPure1nest-fw and CgTure1nest-rv were used to amplify the 3,944-bp urease deletion cassette (Supplementary Fig. S4C). The deletion cassettes were transformed into conidial protoplasts (Werner et al. 2007). Fourteen-day-old cultures were transferred to SYE medium (0.5 M sucrose and 0.1% [wt/vol] yeast extract) supplemented with 10 mM $(NH_4)_2SO_4$ and grown at 23°C and continuous fluorescent light in a BOD 400 incubator (UniEquip; Martinsried, Germany) (Werner et al. 2007). Single-spore isolates were generated by two rounds of conidial dilutions.

To confirm successful deletion of *ALA1* and *URE1* and to test for the frequency of deletion cassette integration, genomic DNA was extracted (Sugui and Deising 2002) and digested with *Hin*dIII (allantoicase deletion) or *Pvu*I (urease deletion), separated by agarose gel electrophoresis, and blotted onto nylon membranes as described above. Blots were hybridized with 443- or 450-bp DIG-dUTP-labeled *ALA1*- or *URE1*-specific probes, which were amplified from genomic DNA of *C. graminicola*, using primers CgAla1probe-fw and CgAla1probe-rv, and CgUre1probe-fw and CgUre1probe-rv. In addition, blots were hybridized with a 474-bp alkali-labile DIG-dUTP-labeled (Roche Diagnostics, Mannheim, Germany) *hph*-specific probe, which was amplified from plasmid pAN7-1 (Punt et al. 1987) using primers HygRprobe-fw and HygRprobe-rv. Hybridization and visualization of the hybridized DIG-dUTP-labeled probe were performed as described (Münch et al. 2011).

**Quantitative PCR.** Fungal development on plants was quantified by quantitative PCR (qPCR) as described (Weihmann et al. 2016). DNA for qPCR analyses was isolated using peqGold Plant DNA Mini Kit (PEQLAB Biotechnologie GmbH, Erlangen, Germany), according to the manufacturer's instructions.

**Microscopy.** Bright field and DIC microscopy was performed with a Nikon Eclipse 600 epifluorescence microscope (Nikon, Düsseldorf, Germany). Digital images were taken with a CCD-1300 camera (VDS Vosskühler GmbH, Osnabrück, Germany). Fluorescence microscopy was done using a Plan Apochromat 60/1.4 oil immersion objective and an AxioCam MRm camera (Carl Zeiss Microscopy GmbH, Jena, Germany). For epi-illumination analyses, the following settings were used: excitation wavelength, 488 nm; laser light transmittance, 25% (ND4 in; ND8 out); and pinhole

diameter, 30 mm, excitation wavelengths and filter set 545/30 nm, and 620/60 nm for *eGFP*.

Image acquisition and analysis were performed using ImageJ software (Schneider et al. 2012).

**Dye inclusion urease activity assays.** Mycelium plugs (Ø 4 mm) excised from 10-day-old cultures were used to inoculate a modified YS agar (BD Difco yeast nitrogen base without amino acids and ammonium sulfate; Fisher Scientific GmbH, Schwerte, Germany) (Dye 1968), containing 0.02 mM bromothymol blue instead of cresol red. Hydrolysis of urea leads to a pH increase. The intensity of blue color of the medium, indicative of urease activity, was evaluated after 5 and 10 days of incubation at 23°C in the dark.

**Phylogenetic and amino acid sequence analyses.** To construct phylogenetic trees for allantoicase and urease, the protein sequences were compared with sequences from specimens available in the GenBank database of NCBI (https://www.ncbi.nlm.nih.gov/), aligned using CLUSTAL W (Higgins et al. 1994) and adjusted using software Mega X (Kumar et al. 2018). Bayesian Inferences were computed with MrBayes 3.2.1 (Ronquist et al. 2012), using the permutations needed to reach split frequencies of less than or equal to 0.01 and discarding the first 25% generated trees. The substitution model LG + G + I was selected and incorporated in the Bayesian analysis. The trees were edited using the software FigTree v.1.3.1 (Rambaut 2010).

## RESULTS

**The single-copy genes *ALA1* and *URE1* of *C. graminicola* code for allantoicase and urease proteins.** BLASTP searches with known allantoicase (EC 3.5.3.4) and urease (EC 3.5.1.5) proteins of *C. higginsianum* and *C. fioriniae* identified the homologous proteins Ala1 and Ure1 in *C. graminicola*. The corresponding single-copy genes discovered in the genome of *C. graminicola* (https://www.broadinstitute.org/annotation/genome/colletotrichum_group/FeatureSearch.html) were designated as *ALA1* (GLRG_07310.1) and *URE1* (GLRG_00633.1). *ALA1* comprises 1,130 bp, with two exons (Fig. 1A), and the enzyme Ala1 consists of 354 amino acids (aa) organized into two allantoicase repeats (pfam03561). Repeat 2 carries a FGKR amidation site (aa 350 to 353) at its C-terminus (Fig. 1B). The urease gene *URE1* consists of 2,832 bp, with five exons (Fig. 1C). The 835-aa Ure1 enzyme is composed of three domains, with the C-terminal α-domain harboring nickel and substrate binding sites, a MVC*H*HLSKNIPEDVAFA proton donor site at the active center, and a KMRVDPESY tyrosine kinase phosphorylation motif (INTERPRO, https://www.ebi.ac.uk/interpro/protein/UniProt/E3Q4H7/) (Fig. 1D). The phylogenetic trees (Fig. 1E and F) based on the Bayesian inference of amino acid sequences follow the six-gene phylogeny of the Kingdom of Fungi (James et al. 2006) and reveal that the Ala1 and Ure1 proteins of *C. graminicola* are both orthologous to Ala1 and Ure1

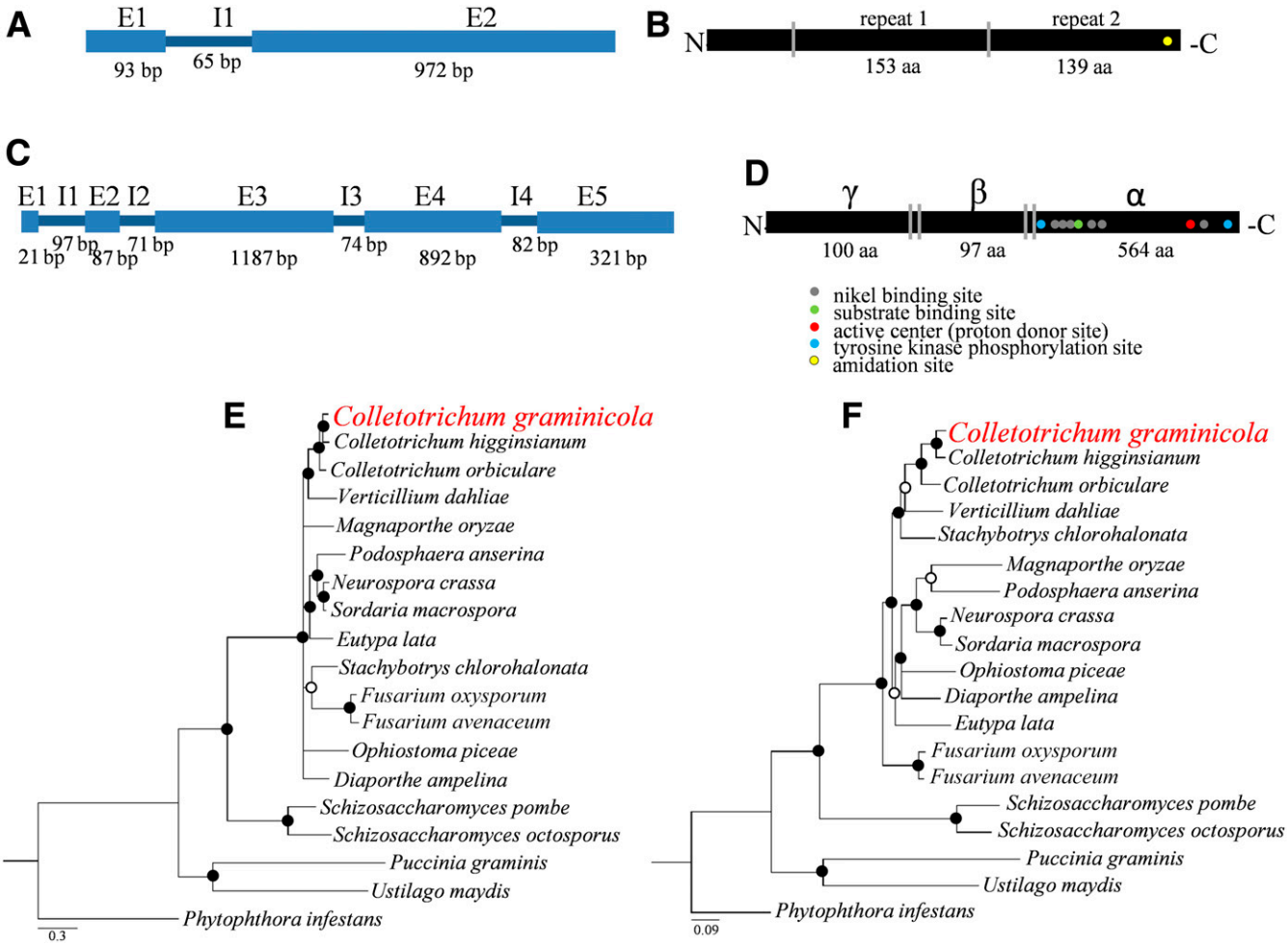


**Fig. 1.** Allantoicase and urease nucleotide and amino acid sequences, and protein phylogeny. **A and C,** Structure of *ALA1* and *URE1* genes. E denotes exons, I denotes introns. Nucleotide numbers are given below blue bars. **B and D,** Ala1 and Ure1 protein structures, respectively. Ala1 consists of two repeats, with repeat 2 harboring an amidation site; and Ure1 consists of three domains, with the C-terminal α domain containing Ni-binding, substrate activation, proton donor, and tyrosine kinase phosphorylation sites. Bayesian inference tree based on protein sequences of **E,** allantoicase and **F,** urease from 19 species available in the GenBank database of NCBI. Circles on the nodes indicate Bayesian posterior probability. Solid circles indicate values equal to or higher than 0.8, and open circles indicate values lower than 0.8. The tree was rooted to the sequence of *Phytophthora infestans*. Scale bars indicate the number of substitutions per site.

described for 14 other Sordariomycetes, two yeast and two Basidiomycetes. The Ala1 and Ure1 proteins of *C. graminicola* share higher similarity with the corresponding proteins of *C. higginsianum* and *C. orbiculare* than with the other Sordariomycetes (Fig. 1E and F). Overall, the close relatedness of the proteins analyzed here is indicated by very low average aa exchange rates, corresponding to 0.3 exchanges per site across the allantoicase sequences and 0.09 exchanges across the urease aa sequences compared here (Fig. 1E and F). In accordance with the eukaryote phylogeny (Cavalier-Smith et al. 2015), the trees also revealed that the allantoicase and urease proteins of *C. graminicola* and of the potato late blight oomycete, *Phytophthora infestans*, are only distant related.

***ALA1* and *URE1* are expressed before host cell invasion and contribute to appressorial penetration and full virulence.** In order to investigate at which stages of pathogenesis *ALA1* and *URE1* are expressed, we generated strains synthesizing C-terminal eGFP fusions to the Ala1 and Ure1 proteins, respectively (Supplementary Fig. S2A to D). Macroscopically, disease symptoms caused by *ALA1*:*eGFP* and *URE1*:*eGFP* strains did not differ from those caused by the WT strain (Supplementary Fig. S2E). As the *ALA1*- and *URE1*-deficient deletion strains Δ*ala1* and Δ*ure1* showed virulence defects (see below), we conclude that eGFP fusions of *ALA1* and *URE1* were functional.

Conidia of *ALA1*:*eGFP* and *URE1*:*eGFP* strains exhibited no fluorescence before, but strong fluorescence after inoculation onto the maize cuticle, i.e., at 0 hpi (Fig. 2, 0 hpi). eGFP fluorescence was detected in germ tubes but was hardly visible in mature melanized appressoria differentiated at 24 hpi (Fig. 2, 24 hpi). At 72 hpi, infection hyphae of *ALA1*:*eGFP* and *URE1*:*eGFP* strains had invaded their host cells and did not show *eGFP* fluorescence, suggesting that expression of these genes and degradation of fungal purines are no longer required when the pathogen had switched to necrotrophy and gained access to plant nitrogen sources. To exclude the possibility that infection hyphae of the *eGFP* fusion strains do not show fluorescence because the light is emitted in deeper mesophyll layers and therefore not visible, we performed infection assays with a $P_{TOXB}$:*eGFP* strain of *C. graminicola*. In this strain, *eGFP* expression is controlled by the strong constitutive *TOXB* promoter of the tan spot fungus *Pyrenophora tritici repentis* (Andrie et al. 2005; Oliveira-Garcia and Deising 2013). In marked contrast to the *ALA1*:*eGFP* and *URE1*:*eGFP* strains, necrotrophic infection hyphae of the $P_{TOXB}$:*eGFP* strain fluoresced strongly in the mesophyll of maize leaves (Fig. 2, 72 hpi, ih), supporting the view that *ALA1* and *URE1* are expressed preferentially at preinvasion stages. The WT strain did not show fluorescence at any stage of pathogenesis (Fig. 2, WT). Also on cellophane layers only preinvasive infection structures of *ALA1*:*eGFP* and *URE1*:*eGFP* strains showed fluorescence (Supplementary Fig. S3), suggesting that expression of *ALA1* and *URE1* is morphogenetically regulated and not controlled by unavailability of nitrogen.

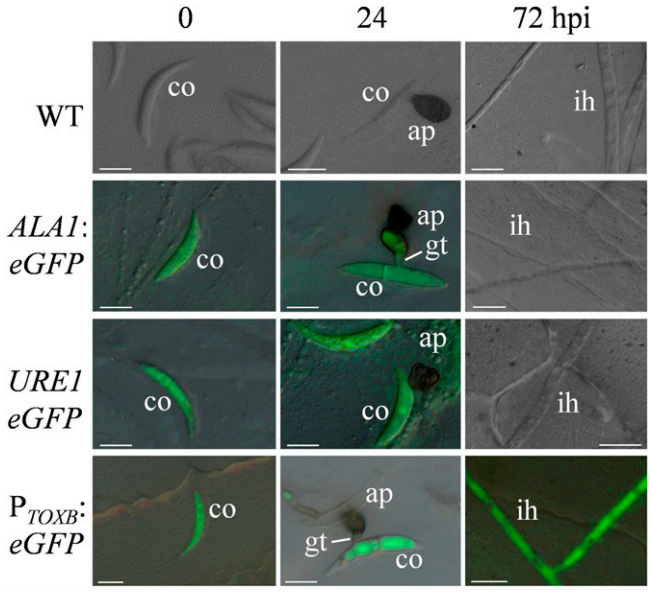


**Fig. 2.** Infection-related expression of *ALA1* and *URE1*. The wild-type (WT), *ALA1:eGFP*, *URE1:eGFP*, and *PTOXB:eGFP* strains were inoculated onto onion epidermal cells and allowed to differentiate infection structures for 72 h. Infection structures were analyzed by differential interference contrast and eGFP-fluorescence microscopy; micrographs shown represent overlays. All assays were performed with three independent mutant strains, with three independent repeats. Representative micrographs are shown. co, conidium; gt, germ tube; ap, appressorium; and ih, infection hypha. Bars are 10 μm.

To functionally characterize *ALA1* and *URE1*, deletion constructs (Supplementary Fig. S4) were transformed into protoplasts of *C. graminicola*. Homologous recombination resulted in replacement of the coding sequence of *ALA1* or *URE1* by the deletion cassette containing the hygromycin phosphotransferase gene (*hph*) of *Escherichia coli* (Supplementary Fig. S4A and C), as indicated by PCR (data not shown) and confirmed by Southern blot analyses (Supplementary Fig. S4B and D). In total, 11 and 4 independent Δ*ala1* and Δ*ure1* deletion strains, and seven and six transformants with an ectopically integrated deletion cassette (ect.) were identified.

Dye (1968) had demonstrated that a pH increase and, thus, a color shift specifically occurred in the presence of a pH indicator when ammonia was enzymatically released from urea. Adopting an *in substratum* urease activity assay for *C. graminicola*, we allowed colonies to grow on yeast nitrogen agar (YNA) containing bromothymol blue (BTB) as a pH indicator and observed color shifts caused by the WT and the ectopic strains. By contrast, Δ*ala1* and Δ*ure1* deletion strains did not cause blue staining of the substratum, suggesting that ammonium was not produced in the absence of *ALA1* or *URE1* (Fig. 3A).

At 3 dpi the WT strain had caused dark necrotic lesions, as typically observed in leaf segment assays (Oliveira-Garcia and Deising 2016). In comparison with the WT strain, Δ*ala1* and Δ*ure1* mutants caused strongly reduced or no disease symptoms at 3 dpi (Fig. 3B). Using internal transcribed spacer 2 (ITS2) primers as described (Weihmann et al. 2016), macroscopically observed virulence defects of Δ*ala1* and Δ*ure1* mutants were fully confirmed by qPCR analyses (Fig. 3C). Mock-inoculated leaves showed no anthracnose disease symptoms, and symptoms caused by transformants carrying an ectopically integrated allantoicase or urease deletion construct were WT-like (Fig. 3B). In order to determine the infection stage at which the mutants are hampered, infection structures were quantified microscopically (Fig. 3D). Δ*ala1* and Δ*ure1* mutant strains germinated and differentiated appressoria at rates similar to the WT strain and appressoria exhibited WT-like shape and melanization. However, appressorial penetration rates on maize epidermal cells and, hence, rates of differentiation of infection hyphae in planta were significantly reduced in both mutants at 48 hpi (Fig. 3D). At this time point, 85% of the appressoria of the WT strain had penetrated the epidermal maize cell wall and formed infection hyphae compared with only 26 and 30% of the appressoria of Δ*ala1* and Δ*ure1* mutants, respectively (Fig. 3D), indicating appressorial penetration deficiencies. After extending the incubation time to 5 days, the disease symptoms caused by Δ*ala1* and Δ*ure1* mutants became more intense and similar to those caused by the WT strain (Fig. 3B and C). Collectively, microscopy and infection assays strongly suggested that Δ*ala1* and Δ*ure1* mutants were hampered by compromised nitrogen availability occurring at the appressorial penetration stage of pathogenesis. Indeed, inoculation of conidia onto wounded leaves, on which plant metabolites, including nitrogen sources, are readily available, showed that Δ*ala1* and Δ*ure1* mutants caused

disease symptoms similar to those caused by the WT and ectopic strain already at 3 dpi (Fig. 3B, 3 dpi wounded).

In order to further confirm that nitrogen unavailability at the appressorial penetration stages of infection, as caused by disruption of the purine degradation pathway, is causal for reduced virulence, we inoculated Δ*ure1* mutants onto intact maize leaves and supplemented the infection droplet with 10 mM $(NH_4)_2SO_4$ (Fig. 4). Interestingly, chemical complementation of the Δ*ure1* mutant increased the symptom intensity at both 3 and 5 dpi, as compared with the noncomplemented mutant. Application of 10 mM $(NH_4)_2SO_4$ alone did neither cause chloroses nor necroses, and $(NH_4)_2SO_4$ is therefore not regarded as phytotoxic on maize leaves at the concentration used (Fig. 4). The increase of symptom intensity by chemical complementation of the Δ*ure1* mutant is in line with the view that purine degradation is required for bridging the prepenetration nitrogen gap and for full virulence.

**Chemical inhibition of urease protects plants from fungal infection.** In contrast to nickel-complexing urease inhibitors, acetohydroxamic acid (AHA) is structurally related to urea, forms stable complexes with but is not hydrolysable by the enzyme urease, and thus acts as a potent and appropriately specific urease inhibitor (Fishbein and Carbone 1965; Kafarski and Talma 2018). Indeed, addition of AHA to the substratum amended with BTB strongly reduced formation of blue color in the medium inoculated with the *C. graminicola* WT strain (Fig. 5A). Thus, in order to test whether inhibition of fungal urease activity would protect maize leaves from infection by the anthracnose fungus, we added 10 mM AHA to the infection droplet. Remarkably, at 3 and 5 dpi anthracnose disease symptoms had not developed. In comparison, in the absence of the urease inhibitor the WT strain of *C. graminicola* caused clear disease symptom at 3 dpi, which became more severe at 5 dpi (Fig. 5B). Moreover, quantification of infection structure differentiation by microscopy showed that the inhibitor-treated and untreated WT strain germinated and differentiated appressoria at similar rates. However, in the presence of AHA appressoria were significantly impaired in

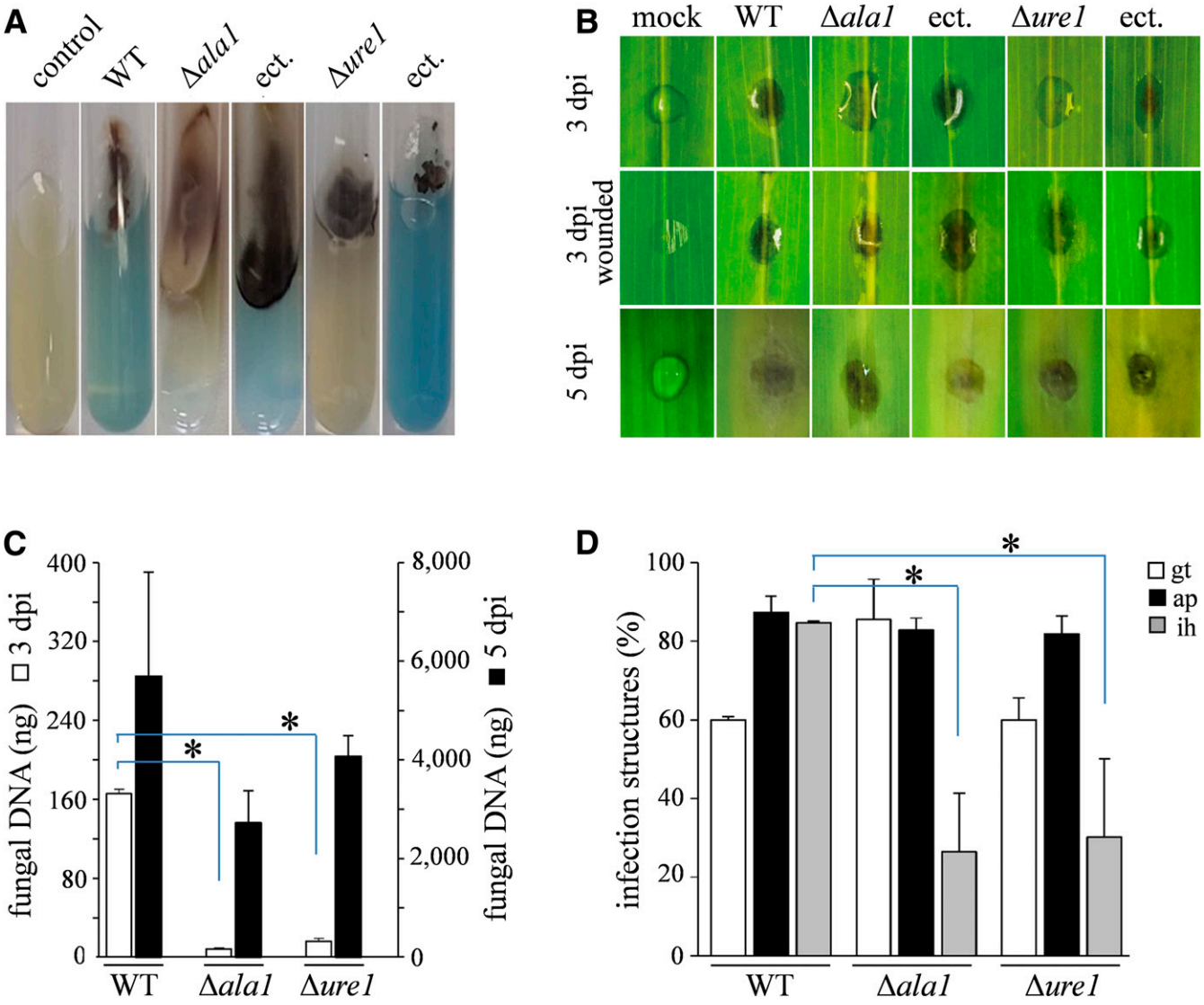


**Fig. 3.** Dye inclusion urease activity assays and virulence assays. **A,** Growth of wild-type (WT), *Δala1*, and *Δure1* strains, and corresponding strains with ectopically integrated deletion cassettes (ect.) on YS agar containing 0.02 mM bromothymol blue. Control is noninoculated substratum. **B,** Infection assays on intact and wounded maize leaf segments. Strains are as described in **A,** mock, leaves treated with 0.02% (vol/vol) Tween 20. Photographs were taken at 3 and 5 days postinoculation (dpi). **C,** Quantification of fungal mass at infection sites by qPCR, with eight inoculation sites grouped per DNA extraction and four repeats. Strains used are those used in **A**. **D,** Infection structure differentiation. gt, germ tubes; ap, appressoria; and ih, infection hyphae. Infection structures were counted at 48 h postinoculation. Percent values relate to the preceding structure. All assays were performed with three independent mutant or ectopic strains, with three independent repeats. **B,** representative infection sites are shown. **C and D,** Error bars are standard deviations and asterisks indicate statistically significant differences at $P \leq 0.01$ using one-way analysis of variance with Tukey's post hoc test.

invading maize epidermal cells, as indicated by formation of only 5% of infection hyphae as compared with 88% in untreated controls at 48 hpi (Fig. 5C). These data show that the hemibiotroph *C. graminicola* requires a functional urease for effective host invasion and suggest that urease inhibitors could be used to interfere with host invasion also of other hemibiotrophs and biotrophs.

We therefore addressed the pathogen specificity of urease inhibition and investigated the infection process of and symptom development caused by pathogens differing in lifestyle and host plant in the presence of AHA. Leaves of winter wheat plants were sprayed with 10 mM AHA, allowed to dry and inoculated with conidia of the biotrophic wheat powdery mildew fungus *B. graminis* f. sp. *tritici*. Mildew-inoculated plants without the inhibitor and noninoculated inhibitor-treated plants served as controls. At 6 dpi, dense mildew pustules had formed on control plants, but pustule development was negligible on AHA-treated leaves at that time point (Fig. 6A) and plants showed only minor mildew disease symptoms at 12 dpi. Leaves sprayed with the inhibitor alone showed neither chloroses nor necroses. Microscopy revealed that conidia (Fig. 6B; *Bgt*, co) had formed primary (Fig. 6B; *Bgt*, pgt) and appressorial germ tubes (Fig. 6B; *Bgt*, agt), which differentiated appressoria (Fig. 6B; *Bgt*, ap). By 48 hpi, appressoria had breached the epidermal cell wall, invaded the wheat cell, and formed haustoria (Fig. 6B; *Bgt*, insert, hau; Fig. 6C). On AHA-treated leaves (Fig. 6B, *Bgt* + AHA), formation of primary and appressorial germ tubes and of appressoria was similar to control leaves, but differentiation of haustoria was significantly reduced (Figs. 6B, *Bgt* + AHA; Fig. 6C). In order to investigate the effect of AHA on biotrophic fungi that employ a distinct infection strategy, we employed rust fungi infecting dicot and monocot hosts, i.e., the broad bean rust fungus *U. viciae-fabae* and the maize rust fungus *Puccinia sorghi*. The majority of rust fungi, including *U. viciae-fabae* and *Puccinia sorghi*, position appressoria on stomatal pores (Hoch et al. 1987) to invade their host leaves and differentiate infection hyphae in the intercellular space, followed by formation of haustorial mother cells and hautoria (Mendgen and Deising 1993). At 12 dpi, successful infection by *U. viciae-fabae* was obvious, as large numbers of uredosori had formed on broad bean leaves (Fig. 6D, *Uvf*). By contrast, when AHA had been added to the urediniospore suspensions used to inoculate the plants, disease symptom development did not occur until the end of the experiment at 12 dpi. As with wheat leaves, AHA alone, at the concentration and time point investigated, did not cause phytotoxic effects. As rust hyphae differentiated in the intercellular space are difficult to visualize, polyethylene sheets with thigmo-inductive ridges (Deising et al. 1991) were inoculated with urediniospores in the presence or absence of AHA. Untreated urediniospores (Fig. 6E, *Uvf*, us) germinated and, after contacting a ridge, differentiated an appressorium (Fig. 6E, *Uvf*, ap), a substomatal vesicle (Fig. 6E, *Uvf*, sv), and an infection hypha (Fig. 6E, *Uvf*, ih), as revealed by differential interference contrast microscopy. In the

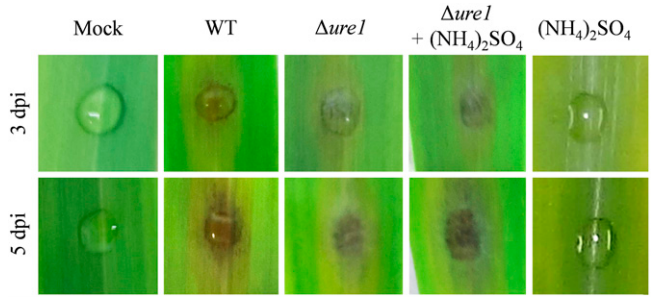


**Fig. 4.** Complementation of virulence defects of *Δure1* strains by $(NH_4)_2SO_4$. Maize leaf segments were inoculated with *Δure1* strains in the absence or presence of 10 mM $(NH_4)_2SO_4$, and disease symptoms were photographed at 3 and 5 days postinoculation (dpi). Infection assays were performed with three independent *Δure1* strains, with three repeats. Mock treatment was done with 0.02% (vol/vol) Tween 20; application of 10 mM $(NH_4)_2SO_4$ did not indicate toxicity. Inoculation with the wild-type (WT) strain served as positive control. Representative infection sites are shown.

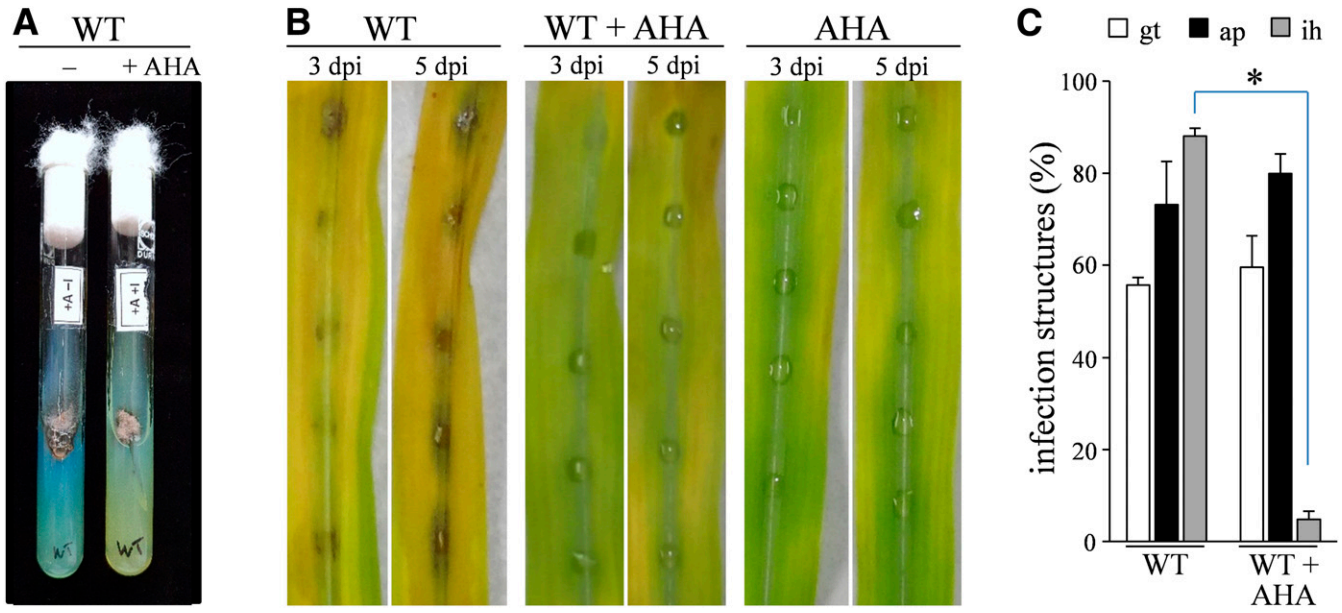


**Fig. 5.** Effect of the urease inhibitor acetohydroxamic acid (AHA) on urease activity and anthracnose disease development on maize leaf segments inoculated with the *Colletotrichum graminicola* wild-type (WT) strain. **A,** Dye inclusion urease activity assays as in Figure 3A. – or + AHA indicates absence or presence of the inhibitor. **B,** Maize leaf segments were inoculated with conidial suspensions without (WT) or containing 10 mM AHA (WT + AHA). At a concentration of 10 mM AHA (AHA), no toxicity was observed. Infected leaves were photographed at 3 and 5 dpi. Representative anthracnose disease symptoms are shown. **C,** Infection structure differentiation in the absence (WT) or presence of the urease inhibitor (WT + AHA). gt, germ tubes; ap, appressoria; and ih, infection hyphae. Infection structures were counted at 48 h postinoculation. Percent values relate to the preceding structure. Error bars are standard deviations. Asterisks indicate statistically significant differences at $P \leq 0.01$ using one-way analysis of variance with Tukey's post hoc test. All assays were performed as three independent repeats.

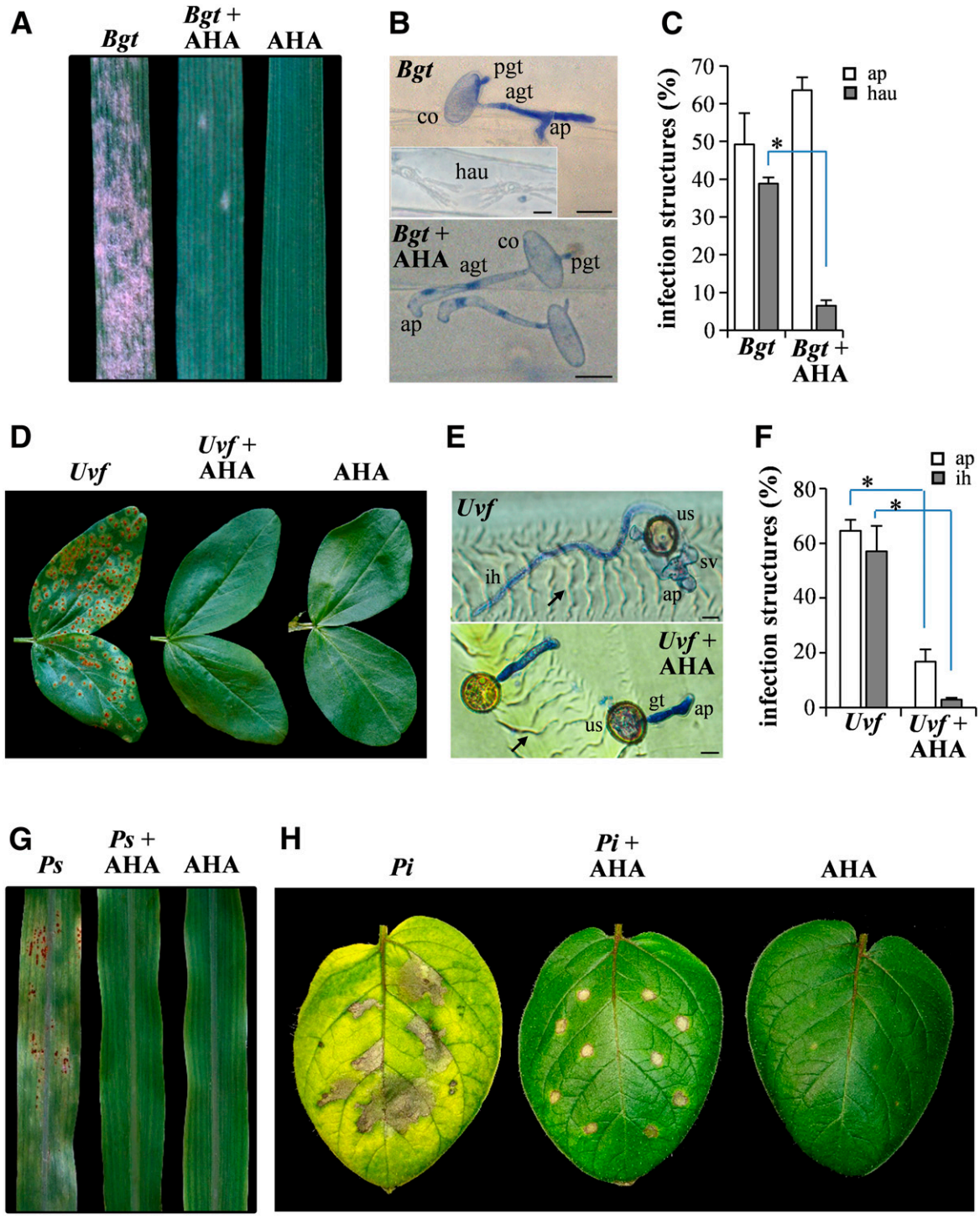


**Fig. 6.** Effect of the urease inhibitor acetohydroxamic acid (AHA) on disease development of biotrophic pathogens and of the potato pathogen *Phytophthora infestans*. **A to C,** Wheat powdery mildew fungus *Blumeria graminis* f. sp. *tritici* (*Bgt*). **A,** Leaves inoculated with *Bgt*, or pretreated with 10 mM AHA and subsequently inoculated with conidia of the wheat powdery mildew fungus (*Bgt* + AHA). Control leaves were only treated with AHA (AHA). Leaves were photographed at 6 days postinoculation (dpi). **B,** Infection structure differentiation on leaves not treated (*Bgt*) or treated with AHA (*Bgt* + AHA). Structures formed on the leaf surface were stained with methyl blue (de Neergaard 1997). Haustoria formed in the host cell are unstained. co, conidium; pgt, primary germ tube; agt, appressorial germ tube; ap, appressorium; hau, haustorium (*Bgt*, insert). Micrographs were taken at 48 h postinoculation (hpi). **C,** Quantification of infection structures differentiated in the absence (*Bgt*) or presence of the urease inhibitor (*Bgt* + AHA). ap, appressoria; and hau, haustoria. Infection structures were counted at 48 hpi. Percent values relate to the preceding structure. Three times 100 infection structures were counted. **D to F,** Broad bean rust fungus *Uromyces viciae-fabae* (*Uvf*). **D,** Leaves were sprayed with urediniospore suspensions (*Uvf*), or urediniospore suspensions containing 10 mM AHA (*Uvf* + AHA). Control leaves were treated with 10 mM AHA (AHA). Leaves were photographed at 12 dpi. **E,** Infection structure differentiation on thigmo-inductive polyethylene sheets. Structures were stained with methyl blue. us, urediniospore; ap, appressorium; sv, substomatal vesicle; and ih, infection hypha. Arrows point at thigmo-inductive ridges. **F,** Quantification of infection structures differentiated in the absence (*Uvf*) or presence of the urease inhibitor (*Uvf* + AHA). ap, appressoria; and ih, infection hypha. Infection structures were counted at 24 hpi. Percent values relate to appressoria. Three times 100 infection structures were counted. **G,** Maize rust fungus *Puccinia sorghi* (*Ps*). Leaves were sprayed with urediniospore suspensions (*Ps*) or urediniospore suspensions containing 10 mM AHA (*Ps* + AHA). Control leaves were treated 10 mM AHA (AHA). Leaves were photographed at 9 dpi. **H,** hemibiotrophic potato late blight oomycete *Phytophthora infestans* (*Pi*). Leaves were inoculated with zoospore suspensions (*Pi*), or zoospore suspensions containing 10 mM AHA (*Pi* + AHA). Control leaves were treated 10 mM AHA only (AHA). Leaves were photographed at 7 dpi. Three independent repeats of the experiments were performed, representative leaves are shown. **C and F,** Error bars are standard deviations and asterisks indicate statistically significant differences at $P \leq 0.01$ using one-way analysis of variance with Tukey's post hoc test.

presence of AHA, germ tubes and, at dramatically reduced rates, appressoria and infection hyphae were formed (Fig. 6E, *Uvf* + AHA; Fig. 6F), clearly indicating that functional urease is also required for infection-related morphogenesis in the broad bean rust fungus. AHA also strongly reduced rust disease symptom severity caused by the maize rust fungus *Puccinia sorghi* (Fig. 6G).

The oomycete and potato late blight pathogen *Phytophthora infestans* is more closely related to chromophyte algae, and thus to plants than to fungi (Cavalier-Smith 2018; Cavalier-Smith et al. 2015). At 5 dpi, the oomycete had caused massive chloroses and beginning necroses on potato leaves in the absence of the urease inhibitor (Fig. 6H, *Pi*). The urease inhibitor did not completely obliterate late blight infection, but symptom development had stopped at 5 dpi and remained unaltered until 14 dpi, with distinct necrotic zones surrounding the infection sites and growth restriction of the pathogen (Fig. 6H, *Pi* + AHA). In the absence of the pathogen, the inhibitor occasionally caused minor water-soaked lesions on potato leaves, indicative of some toxic potential of AHA at the concentration and the experimental conditions used.

## DISCUSSION

Inspired by the observation that an ATMT mutant of *C. graminicola*, carrying a T-DNA integration within the promoter region of the *ALA1* gene, was impaired in virulence (Münch et al. 2011), we decided to investigate the importance of the key genes of the purine degradation pathway, *ALA1* and *URE1*, of the maize anthracnose fungus in more detail. In spite of the fact that the prepenetration phase of the fungal infection process is thought to be particularly nitrogen-demanding (Soanes et al. 2012), the role of purine degradation in nitrogen reallocation is still largely unknown.

The targeted mutagenesis experiments reported here show that *ALA1* and *URE1* of *C. graminicola* are required for plant invasion and efficient establishment of a compatible interaction with the host plant. Employing the chemical urease inhibitor AHA suggested that functional urease is not only required for the infection process of the maize anthracnose fungus, but also for biotrophic fungi causing powdery mildew of wheat, rust in maize and broad bean and for the taxonomically distant hemibiotrophic oomycete *Phytophthora infestans*. Thus, our molecular genetics experiments led to identifying a metabolic inhibitor class, so far used to improve nitrogen fertilizer efficiency (Fu et al. 2020), as a compound contributing to plant health. Importantly, as the urease inhibitor used does not kill the pathogens it cannot be regarded as fungicidal, which may be of relevance in legislation and designing of novel plant health strategies.

In marked contrast to its role in fungal pathogens of plants, urease has been identified as a major virulence factor in several mammalian pathogens, including bacteria such as *Helicobacter pylori* and *Proteus mirabilis*, and filamentous fungi like the ascomycete *Coccioides posadasii*, the basidiomycete *Cryptococcus neoformans*, and others (Mora and Arioli 2014). Significant interest in the role of urease in pathogenesis was raised by the discovery that the bacterium *H. pylori* is associated with the occurrence of gastritis and stomach cancer. *H. pylori* grows at pH values between 6 and 8 and is rapidly killed at pH values below 4. The persistence of the bacterium in the stomach critically depends on the enzyme urease, which, in the presence of urea, can liberate ammonia and thus increase the pH to neutral levels or even above, and urease-based pH adaptation and establishment of a hostile microenvironment is mechanistically indispensable for disease establishment (Burne and Chen 2000; Weeks et al. 2000). Moreover, a urease deficient mutant of *Proteus mirabilis*, the causal agent of bacteriuria and acute pyelonephritis in humans, showed a 1,000-fold greater 50% infective dose than the parental strain, indicating that urease is a virulence factor also in this bacterium (Johnson et al. 1993).

The importance of urease-dependent increase of microenvironmental pH has not only been reported in the stomach-inhabiting bacterium *H. pylori*. Likewise, in the respiratory dimorphic fungus *Coccidioides posadasii* urease activity is necessary for increasing the pH in infected lung tissue, and a urease-deficient mutant strain of this fungus had significant virulence defects, possibly due to their inability of active pH adjustment (Mirbod-Donovan et al. 2006). Moreover, urease-deficient strains of the dimorphic basidiomycete and human pathogen *Cryptococcus neoformans* were significantly reduced in virulence, as indicated by lower cryptococcal loads in brains of mice inoculated with the urease-deficient strain, as compared with the WT. Interestingly, while direct inoculation of WT and urease-deficient mutants into mural brains suggested that urease was not required for growth in the brain tissue, dissemination patterns in the brain, spleen, and other organs differed clearly after intravenous inoculation, strongly suggesting a role of urease in facilitating blood-to-brain invasion in this fungus (Olszewski et al. 2004; Shi et al. 2010). Whether or not alkalinizing is functionally required for blood-to-brain invasion by *Cryptococcus neoformans* is unclear.

In contrast to invasive human pathogens such as *Candida albicans*, *Aspergillus fumigatus*, and *Cryptococcus neoformans*, which have direct access to the abundant nitrogen sources of their hosts (Chitty and Fraser 2017), the plant surface is poor in nitrogen (Buschhaus and Jetter 2011; Podila et al. 1993), making purine degradation and urease-mediated ammonium release important at early phases of plant infection. In biotrophic and hemibiotrophic plant pathogenic fungi alkalinization of the microenvironment has not been reported. The data presented here propose a novel functional role of urease and, possibly, of the purine degradation pathway in biotrophic and hemibiotrophic plant pathogenic fungi.

Depending on the mode of infection, nitrogen limitation may not only occur on the plant surface but also in specific tissue types within the host. For example, the root-invading wilt fungus *F. oxysporum* colonizes its host through nitrogen-deprived xylem vessels. In this fungus, disruption of the global nitrogen regulator gene *FNR1*, which is required for adaptation to nitrogen limitation, strongly reduced its ability to use secondary nitrogen sources such as uric acid and hypoxanthine, and mutants showed a clear delay in disease progression in infection assays on tomato seedlings. Interestingly, transcript abundance of the urate oxidase (syn. uricase) gene was dramatically reduced in *FNR1* disruption mutants (Divon et al. 2006). Correspondingly, mutants of the bean pathogen *Colletotrichum lindemuthianum* lacking the *FNR1* homolog *CLNR1*, were unable to grow on substrata containing urea as the sole nitrogen source, and were strongly impaired in virulence (Pellier et al. 2003).

As most if not all genomes of fungal leaf pathogens harbor genes for purine degradation, including urease-encoding genes, we reasoned that urease inhibitors might prevent or delay plants infections. Treatment of economically relevant pathogens such as the maize anthracnose fungus *C. graminicola*, the powdery mildew fungus *B. graminis* f. sp. *tritici*, as well as the rust species *Puccinia sorghi* and *U. viciae-fabae*, with the urease inhibitor AHA strongly reduced disease symptoms. In comparison, AHA only partially inhibited *Phytophthora infestans* infection of potato leaves, but initial spread of the pathogen was restricted, suggesting that urease inhibitors might affect even distantly related pathogens.

Collectively, the genetic data shown here indicate that *ALA1* and *URE1* are required for full virulence of the maize anthracnose fungus *C. graminicola*. The role of urease at early infection stages, as shown by gene deletion studies, was confirmed by chemical inhibition of urease activity in hemibiotrophic and biotrophic pathogens infecting mono- and dicot crops. The experiments presented here are an example of how molecular data can be used to improve plant health strategies.

**Accession numbers.** Fungal allantoicase amino acid sequences can be found under the following National Center for Biotechnology information (NCBI; https://www.ncbi.nlm.nih.gov/) accession numbers: *C. graminicola*: EFQ32166.1; *C. higginsianum*: TIC96856.1; *C. orbiculare*: TDZ23010.1; *M. oryzae*: EHA56801.1; *Podospora anserina*: CDP27419.1; *Stachybotrys chlorohalonata*: KFA63776.1; *Verticillium dahliae*: EGY22472.1; *Ophiostoma piceae*: EPE03208.1; *Eutypa lata*: EMR72671.1; *F. oxysporum*: EWZ02429.1; *Neurospora crassa*: XP_956494.1; *Sordaria macrospora*: XP_003350828.1; *Diaporthe ampelina*: KKY38077.1; *Fusarium avenaceum*: KIL91383.1; *Schizosaccharomyces pombe*: NP_594495.1; *Schizosaccharomyces octosporus*: XP_013016903.1; *Puccinia graminis*: NP_594495.1; *Ustilago maydis*: KIS70774.1; and *P. infestans*: EEY57616.1.

Fungal urease amino acid sequences can be found under the following accession numbers: *C. graminicola*: EFQ25489.1; *C. higgisianum*: TID07140.1; *C. orbiculare*: TDZ20498.1; *M. oryzae*: ELQ69223.1; *P. anserina*: CDP23462.1; *S. chlorohalonata*: KFA60364.1; *V. dahliae*: EGY17245.1; *O. piceae*: EPE08642.1; *E. lata*: EMR69506.1; *F. oxysporum*: EWZ51967.1; *N. crassa*: KHE85978.1; *S. macrospora*: XP_003348361.1; *D. ampelina*: KKY30255.1; *F. avenaceum*: KIL84477.1; *S. pombe*: NP_594813.1; *S. octosporus*: XP_013018470.1; *P. graminis*: EFP78028.2; *U. maydis*: KIS65956.1; and *P. infestans*: EEY58029.1.

Plasmid pSH1.6EGFP is available under Addgene deposit number 69980.

## ACKNOWLEDGMENTS

We are indebted to Ms. Elke Vollmer, MLU Halle, Germany, for excellent technical assistance and help with plants, Kurt Mendgen, University of Constance, Germany, for providing urediniospores of *U. viciae-fabae* and *P. sorghi*, and Sabine Rosahl, IPB Halle, Germany, for providing *P. infestans* strain CRA208m2. We thank Jorrit-Jan Krijger, MLU Halle, Germany, for stimulating discussions, suggestions and help with the experiments.

## LITERATURE CITED

Andrie, R. M., Martinez, J. P., and Ciuffetti, L. M. 2005. Development of *ToxA* and *ToxB* promoter-driven fluorescent protein expression vectors for use in filamentous ascomycetes. Mycologia 97:1152-1161.

Bechinger, C., Giebel, K.-F., Schnell, M., Leiderer, P., Deising, H. B., and Bastmeyer, M. 1999. Optical measurements of invasive forces exerted by appressoria of a plant pathogenic fungus. Science 285:1896-1899.

Bergstrom, G. C., and Nicholson, R. L. 1999. The biology of corn anthracnose. Knowledge to exploit for improved management. Plant Dis. 83:596-608.

Brown, T. 1999. Southern blotting. Pages 2.9.1-2.9.15 in: Current Protocols in Molecular Biology. F. M. Ausubel, R. Brent, R. E. Kingston, D. D. Moore, J. G. Seidman, J. A. Smith, and K. Struhl, eds. John Wiley & Sons, New York.

Burne, R. A., and Chen, Y. Y. 2000. Bacterial ureases in infectious diseases. Microbes Infect. 2:533-542.

Buschhaus, C., and Jetter, R. 2011. Composition differences between epicuticular and intracuticular wax substructures: How do plants seal their epidermal surfaces? J. Exp. Bot. 62:841-853.

Cavalier-Smith, T. 2018. Kingdom Chromista and its eight phyla: A new synthesis emphasizing periplastid protein targeting, cytoskeletal and periplastid evolution, and ancient divergences. Protoplasma 255:297-357.

Cavalier-Smith, T., Chao, E. E., and Lewis, R. 2015. Multiple origins of Heliozoa from flagellate ancestors: New cryptist subphylum Corbihelia, superclass Corbistoma, and monophyly of Haptista, Cryptista. Hacrobia Chromista. Mol. Phyl. Evol. 93:331-362.

Chitty, J. L., and Fraser, J. A. 2017. Purine acquisition and synthesis by human fungal pathogens. Microorganisms 5:33.

de Neergaard, E. (ed.) 1997. Methods in Botanical Histopathology. Kandrups Bogtrykkeri, Copenhagen, DK.

Deising, H., Jungblut, P. R., and Mendgen, K. 1991. Differentiation-related proteins of the broad bean rust fungus *Uromyces viciae-fabae*, as revealed by high resolution two-dimensional polyacrylamide gel electrophoresis. Arch. Microbiol. 155:191-198.

Divon, H. H., and Fluhr, R. 2007. Nutrition acquisition strategies during fungal infection of plants. FEMS Microbiol. Lett. 266:65-74.

Divon, H. H., Ziv, C., Davydov, O., Yarden, O., and Fluhr, R. 2006. The global nitrogen regulator, FNR1, regulates fungal nutrition-genes and fitness during *Fusarium oxysporum* pathogenesis. Mol. Plant Pathol. 7:485-497.

Dye, D. W. 1968. A taxonomic study of the genus *Erwinia*. 1. The "*amylovora*" group. N.Z. J. Sci. 11:590-607.

Eschen-Lippold, L., Rothe, G., Stumpe, M., Göbel, C., Feussner, I., and Rosahl, S. 2007. Reduction of divinyl ether-containing polyunsaturated fatty acids in transgenic potato plants. Phytochemistry 68:797-801.

Fishbein, W., and Carbone, P. 1965. Urease catalysis. ii. Inhibition of the enzyme by hydroxyurea, hydroxylamine, and acetohydroxamic acid. J. Biol. Chem. 240:2407-2414.

Fu, Q., Abadie, M., Blaud, A., Carswell, A., Misselbrook, T. H., Clark, I. M., and Hirsch, P. R. 2020. Effects of urease and nitrification inhibitors on soil N, nitrifier abundance and activity in a sandy loam soil. Biol. Fertil. Soils 56:185-194.

Halim, V. A., Eschen-Lippold, L., Altmann, S., Birschwilks, M., Scheel, D., and Rosahl, S. 2007. Salicylic acid is important for basal defense of *Solanum tuberosum* against *Phytophthora infestans*. Mol. Plant-Microbe Interact. 20:1346-1352.

Higgins, D., Thompson, J., Gibson, T., Thompson, J. D., Higgins, D. G., and Gibson, T. J. 1994. CLUSTAL W: Improving the sensitivity of progressive multiple sequence alignment through sequence weighting, position-specific gap penalties and weight matrix choice. Nucleic Acids Res. 22: 4673-4680.

Hoch, H. C., Staples, R. C., Whitehead, B., Comeau, J., and Wolf, E. D. 1987. Signaling for growth orientation and cell differentiation by surface topography in *Uromyces*. Science 235:1659-1662.

Horbach, R., Graf, A., Weihmann, F., Antelo, L., Mathea, S., Liermann, J. C., Opatz, T., Thines, E., Aguirre, J., and Deising, H. B. 2009. Sfp-type 4′-phosphopantetheinyl transferase is indispensable for fungal pathogenicity. Plant Cell 21:3379-3396.

James, T. Y., Kauff, F., Schoch, C. L., Matheny, P. B., Hofstetter, V., Cox, C. J., Celio, G., Gueidan, C., Fraker, E., Miadlikowska, J., Lumbsch, H. T., Rauhut, A., Reeb, V., Arnold, A. E., Amtoft, A., Stajich, J. E., Hosaka, K., Sung, G. H., Johnson, D., O'Rourke, B., Crockett, M., Binder, M., Curtis, J. M., Slot, J. C., Wang, Z., Wilson, A. W., Schüssler, A., Longcore, J. E., O'Donnell, K., Mozley-Standridge, S., Porter, D., Letcher, P. M., Powell, M. J., Taylor, J. W., White, M. M., Griffith, G. W., Davies, D. R., Humber, R. A., Morton, J. B., Sugiyama, J., Rossman, A. Y., Rogers, J. D., Pfister, D. H., Hewitt, D., Hansen, K., Hambleton, S., Shoemaker, R. A., Kohlmeyer, J., Volkmann-Kohlmeyer, B., Spotts, R. A., Serdani, M., Crous, P. W., Hughes, K. W., Matsuura, K., Langer, E., Langer, G., Untereiner, W. A., Lücking, R., Büdel, B., Geiser, D. M., Aptroot, A., Diederich, P., Schmitt, I., Schultz, M., Yahr, R., Hibbett, D. S., Lutzoni, F., McLaughlin, D. J., Spatafora, J. W., and Vilgalys, R. 2006. Reconstructing the early evolution of Fungi using a six-gene phylogeny. Nature 443:818-822.

Johnson, D. E., Russell, R. G., Lockatell, C. V., Zulty, J. C., Warren, J. W., and Mobley, H. L. 1993. Contribution of *Proteus mirabilis* urease to persistence, urolithiasis, and acute pyelonephritis in a mouse model of ascending urinary tract infection. Infect. Immun. 61:2748-2754.

Kafarski, P., and Talma, M. 2018. Recent advances in design of new urease inhibitors: A review. J. Adv. Res. 13:101-112.

Käfer, E. 1977. Meiotic and mitotic recombination in *Aspergillus* and its chromosomal aberrations. Adv. Genet. 19:33-131.

Kankanala, P., Czymmek, K., and Valent, B. 2007. Roles for rice membrane dynamics and plasmodesmata during biotrophic invasion by the blast fungus. Plant Cell 19:706-724.

Kleemann, J., Rincon-Rivera, L. J., Takahara, H., Neumann, U., Ver, E., van Themaat, L., van der Does, H. C., Hacquard, S., Stüber, K., Will, I., Schmalenbach, W., Schmelzer, E., and O'Connell, R. J. 2012. Sequential delivery of host-induced virulence effectors by appressoria and intracellular hyphae of the phytopathogen *Colletotrichum higginsianum*. PLoS Pathog 8: e1002643.

Kumar, S., Stecher, G., Peterson, D., and Tamura, K. 2018. MEGA X: Molecular Evolutionary genetics analysis across computing platforms. Mol. Biol. Evol. 35:1547-1549.

Kwaaitaal, M., Nielsen, M. E., Böhlenius, H., and Thordal-Christensen, H. 2017. The plant membrane surrounding powdery mildew haustoria shares properties with the endoplasmic reticulum membrane. J. Exp. Bot. 68: 5731-5743.

Lee, I. R., Yang, L., Sebetso, G., Allen, R., Doan, T. H. N., Blundell, R., Lui, E. Y. L., Morrow, C. A., and Fraser, J. A. 2013. Characterization of the complete uric acid degradation pathway in the fungal pathogen *Cryptococcus neoformans*. PLoS One 8:e64292.

Lee, Y.-H., and Dean, R. A. 1994. Hydrophobicity of contact surface induces appressorium formation of *Magnaporthe grisea*. FEMS Microbiol. Lett. 115:71-76.

Ludwig, N., Löhrer, M., Hempel, M., Mathea, S., Schliebner, I., Menzel, M., Kiesow, A., Schaffrath, U., Deising, H. B., and Horbach, R. 2014. Melanin

is not required for turgor generation but enhances cell wall rigidity in appressoria of the corn pathogen *Colletotrichum graminicola*. Mol. Plant-Microbe Interact. 27:315-327.

Mendgen, K., and Deising, H. 1993. Infection structures of fungal plant pathogens—A cytological and physiological evaluation. New Phytol. 124: 193-213.

Mirbod-Donovan, F., Schaller, R., Hung, C. Y., Xue, J., Reichard, U., and Cole, G. T. 2006. Urease produced by *Coccidioides posadasii* contributes to the virulence of this respiratory pathogen. Infect. Immun. 74:504-515.

Mora, D., and Arioli, S. 2014. Microbial urease in health and disease. PLoS Pathog 10:e1004472.

Münch, S., Ludwig, N., Floß, D. S., Sugui, J. A., Koszucka, A. M., Voll, L. M., Sonnewald, U., and Deising, H. B. 2011. Identification of virulence genes in the corn pathogen *Colletotrichum graminicola* by *Agrobacterium tumefaciens*-mediated transformation. Mol. Plant Pathol. 12:43-55.

Nishimura, S., and Kohmoto, K. 1983. Host-specific toxins and chemical structures from *Alternaria* species. Annu. Rev. Phytopathol. 21:87-116.

O'Connell, R. J., Thon, M. R., Hacquard, S., Amyotte, S. G., Kleemann, J., Torres, M. F., Damm, U., Buiate, E. A., Epstein, L., Alkan, N., Altmuller, J., Alvarado-Balderrama, L., Bauser, C. A., Becker, C., Birren, B. W., Chen, Z., Choi, J., Crouch, J. A., Duvick, J. P., Farman, M. A., Gan, P., Heiman, D., Henrissat, B., Howard, R. J., Kabbage, M., Koch, C., Kracher, B., Kubo, Y., Law, A. D., Lebrun, M. H., Lee, Y. H., Miyara, I., Moore, N., Neumann, U., Nordstrom, K., Panaccione, D. G., Panstruga, R., Place, M., Proctor, R. H., Prusky, D., Rech, G., Reinhardt, R., Rollins, J. A., Rounsley, S., Schardl, C. L., Schwartz, D. C., Shenoy, N., Shirasu, K., Sikhakolli, U. R., Stuber, K., Sukno, S. A., Sweigard, J. A., Takano, Y., Takahara, H., Trail, F., van der Does, H. C., Voll, L. M., Will, I., Young, S., Zeng, Q., Zhang, J., Zhou, S., Dickman, M. B., Schulze-Lefert, P., Ver Loren van Themaat, E., Ma, L. J., and Vaillancourt, L. J. 2012. Lifestyle transitions in plant pathogenic *Colletotrichum* fungi deciphered by genome and transcriptome analyses. Nat. Genet. 44:1060-1065.

Oliveira-Garcia, E., and Deising, H. B. 2013. Infection structure-specific expression of β-1,3-glucan synthase is essential for pathogenicity of *Colletotrichum graminicola* and evasion of β-glucan-triggered immunity. Plant Cell 25:2356-2378.

Oliveira-Garcia, E., and Deising, H. B. 2016. Attenuation of PAMP-triggered immunity in maize requires down-regulation of the key β-1,6-glucan synthesis genes KRE5 and KRE6 in biotrophic hyphae of *Colletotrichum graminicola*. Plant J. 87:355-375.

Olszewski, M. A., Noverr, M. C., Chen, G. H., Toews, G. B., Cox, G. M., Perfect, J. R., and Huffnagle, G. B. 2004. Urease expression by *Cryptococcus neoformans* promotes microvascular sequestration, thereby enhancing central nervous system invasion. Am. J. Pathol. 164: 1761-1771.

Pellier, A. L., Lauge, R., Veneault-Fourrey, C., and Langin, T. 2003. CLNR1, the AREA/NIT2-like global nitrogen regulator of the plant fungal pathogen *Colletotrichum lindemuthianum* is required for the infection cycle. Mol. Microbiol. 48:639-655.

Podila, G. K., Rogers, L. M., and Kolattukudy, P. E. 1993. Chemical signals from avocado surface wax trigger germination and appressorium formation in *C. gloeosporioides*. Plant Physiol. 103:267-272.

Politis, D. J., and Wheeler, H. 1973. Ultrastructural study of the penetration of maize leaves by *Colletotrichum graminicola*. Physiol. Plant Pathol. 3: 465-471.

Punt, P. J., Oliver, R. P., Dingemanse, M. A., Pouwels, P. H., and van den Hondel, C. A. 1987. Transformation of *Aspergillus* based on the hygromycin B resistance marker from *Escherichia coli*. Gene 56:117-124.

Ramazzina, I., Costa, R., Cendron, L., Berni, R., Peracchi, A., Zanotti, G., and Percudani, R. 2010. An aminotransferase branch point connects purine catabolism to amino acid recycling. Nat. Chem. Biol. 6:801-806.

Rambaut, A. 2010. FigTree v1.3.1. Institute of Evolutionary Biology, University of Edinburgh, Edinburgh. http://tree.bio.ed.ac.uk/software/figtree/

Ronquist, F., Teslenko, M., van der Mark, P., Ayres, D. L., Darling, A., Höhna, S., Larget, B., Liu, L., Suchard, M. A., and Huelsenbeck, J. P. 2012. MrBayes 3.2: Efficient Bayesian phylogenetic inference and model choice across a large model space. Syst. Biol. 61:539-542.

Schjoerring, J. K., Husted, S., Mäck, G., and Mattsson, M. 2002. The regulation of ammonium translocation in plants. J. Exp. Bot. 53:883-890.

Schneider, C. A., Rasband, W. S., and Eliceiri, K. W. 2012. NIH Image to ImageJ: 25 years of image analysis. Nat. Methods 9:671-675.

Shi, M., Li, S. S., Zheng, C., Jones, G. J., Kim, K. S., Zhou, H., Kubes, P., and Mody, C. H. 2010. Real-time imaging of trapping and urease-dependent transmigration of *Cryptococcus neoformans* in mouse brain. J. Clin. Invest. 120:1683-1693.

Si-Ammour, A., Mauch-Mani, B., and Mauch, F. 2003. Quantification of induced resistance against *Phytophthora* species expressing GFP as a vital marker: β-aminobutyric acid but not BTH protects potato and *Arabidopsis* from infection. Mol. Plant Pathol. 4:237-248.

Soanes, D. M., Chakrabarti, A., Paszkiewicz, K. H., Dawe, A. L., and Talbot, N. J. 2012. Genome-wide transcriptional profiling of appressorium development by the rice blast fungus *Magnaporthe oryzae*. PLoS Pathog 8: e1002514.

Sugui, J. A., and Deising, H. B. 2002. Isolation of infection-specific sequence tags expressed during early stages of maize anthracnose disease development. Mol. Plant Pathol. 3:197-203.

Talbot, N. J., McCafferty, H. R. K., Ma, M., Moore, K., and Hamer, J. E. 1997. Nitrogen starvation of the rice blast fungus *Magnaporthe grisea* may act as an environmental cue for disease symptom expression. Physiol. Mol. Plant Pathol. 50:179-195.

Tudzynski, B. 2014. Nitrogen regulation of fungal secondary metabolism in fungi. Front. Microbiol. 5:656.

Voegele, R. T., and Mendgen, K. 2003. Rust haustoria: Nutrient uptake and beyond. New Phytol. 159:93-100.

Weeks, D. L., Eskandari, S., Scott, D. R., and Sachs, G. 2000. A $H^+$-gated urea channel: The link between *Helicobacter pylori* urease and gastric colonization. Science 287:482-485.

Weihmann, F., Eisermann, I., Becher, R., Krijger, J.-J., Hübner, K., Deising, H. B., and Wirsel, S. G. R. 2016. Correspondence between symptom development of *Colletotrichum graminicola* and fungal biomass, quantified by a newly developed qPCR assay, depends on the maize variety. BMC Microbiol. 16:94.

Werner, S., Sugui, J. A., Steinberg, G., and Deising, H. B. 2007. A chitin synthase with a myosin-like motor domain is essential for hyphal growth, appressorium differentiation and pathogenicity of the maize anthracnose fungus *Colletotrichum graminicola*. Mol. Plant-Microbe Interact. 20: 1555-1567.

Yu, J. H., Hamari, Z., Han, K. H., Seo, J. A., Reyes-Domínguez, Y., and Scazzocchio, C. 2004. Double-joint PCR: A PCR-based molecular tool for gene manipulations in filamentous fungi. Fungal Genet. Biol. 41:973-981.